The Delayed Response of Airborne Thermometers: Part 3: Measuring the Flux of Sensible Heat

William A. Cooper and others...

DRAFT March 2020

National Center for Atmospheric Research
Earth Observing Laboratory
Research Aviation Facility

Table of Contents

List of Figures

List of Tables

Preface and Abstract

The predecessor papers in this series, Parts 1 and 2, characterized the time response of some airborne thermometers, developed correction procedures for those measurements based on their parameterized transfer functions, and developed a way to correct for the errors introduced when the standard dynamic-heating correction is applied without filtering that signal to match the time response of the sensors. This paper considers the implications of those results for measurements of the flux of sensible heat. In particular, it is showm that one sensor in common use, the unheated Rosemount 102E4AL sensor, will miss important parts of the flux if there are significant contributions above about 1 Hz, but the flux cospectrum can be corrected reliably to extend that limit to near 10 Hz. For examples of measured fluxes, the correction procedure indicates that without this correction the flux measurement would be too small by about 25%. The correction procedure consists of dividing the Fourier transform of the temperature by the transfer function for the temperature sensor before calculating the cospectrum of temperature and vertical-wind fluctuations. Simulation results support the validity of the correction procedure.

Acknowledgments

This material is based upon work supported by the National Center for Atmospheric Research, which is a major facility sponsored by the National Science Foundation under Cooperative Agreement No. 1852977. Any opinions, findings and conclusions or recommendations expressed in this publication are those of the author(s) and do not necessarily reflect the views of the National Science Foundation. The data used in the examples presented are from the VOCALS (VAMOS Ocean-Cloud-Atmosphere-Land Study), SOCRATES (Southern Ocean Clouds, Radiation, Aerosol Transport Experimental Study) and the CSET (Cloud Systems Evolution in the Trades) experiment, each described at this URL. Citations for the data sets are included in the references. Measurements (UCAR/NCAR - Earth Observing Laboratory [2011], UCAR/NCAR - Earth Observing Laboratory [2019], UCAR/NCAR - Earth Observing Laboratory [2018]) were collected by the project experiment teams, and flight operations and data acquisition and processing were performed by the Research Aviation Facility, Earth Observing Laboratory, National Center for Atmospheric Research (NCAR). The analyses reported here were mostly performed using R (R Core Team [2019]), with RStudio (RStudio [2009]) and knitr (Xie [2013, 2014]). Data files in netCDF format have been read and written using the R package "ncdf4"; cf. Pierce [2015]. Substantial use also was made of the "ggplot2" package (Wickham [2009]) for R, and some fits relied on the "nleqslv" package for R Hasselman [2018]. Extensive use was made of the "stats" package, part of Core R. Some of the numerical integrations used the Runge-Kutta function from the "rmutil" package (Swihart and Lindsey [2019]).

1 Introduction

1.1 Overview

As introduced in Part 1, the basis for eddy-correlation measurement of sensible-heat flux (F_s) is the following equation:

$$F_s = \rho_a \, C_p \, \langle w'T' \rangle \tag{1}$$

where ρ_a is the density of air, C_p the specific heat of air at constant pressure, w the vertical wind, and T the temperature. Primes in this equation denote fluctuations from the mean and angle brackets denote an ensemble average. The measurement thus depends on having a temperature sensor that can respond to the range of fluctuations making significant contributions to the heat flux. This measurement requires that temperature be measured with sufficient response to resolve the spectrum of contributions to the flux, and most sensors in routine use are marginal or inadequate for this use. This third paper in a three-part series argues that application of a correction procedure improves this measurement sufficiently to make it reliable despite the response-characteristics of airborne thermometers, at least for one sensor in common use. This paper relies on information from the first two and will need to reference those results in many places.

A crucial characteristic of the temperature sensor is its transfer function, or the ratio of output to input. In particular, as represented as a frequency-dependent function, the transfer function specifies the amplitude and phase of the output for a unit magnitude sinusoidal input of a given frequency. In Part 1, this transfer function was determined by observing the sensor response to measured fluctuations in dynamic heating in regions where those fluctuations were the dominant source of variability in the recovery temperature T_r, which is related to the ambient temperature T_a and the dynamic heating Q according to the equation $T_r = T_a + Q$. The focus in Part 1 was on the relationship between the measured recovery temperature T_m and the true recovery temperature T_r, while Part 2 focused on correcting Q for the response of the sensor to avoid the introduction of noise and false variations arising from fluctuations in dynamic heating to which the temperature sensor cannot respond. Here the key results from those first two papers will be used: (i) the transfer function $H(\nu)$ as a function of frequency ν; and (ii) the modified dynamic-heating term Q' obtained by filtering Q according to the sensor response characteristics.

1.2 Outline of the correction procedure

Two approaches are presented. Both follow the steps below but differ in step 2:

1. Find the transfer function. The estimated air temperature is normally calculated from $T_a = T_m - Q$ where T_m is the measured recovery temperature, but here it is desired to correct both T_m and Q on the basis of the known transfer function

$H(\nu)$. The first step is therefore to determine an appropriate transfer function. In Part 1, it was argued that the result varies with Mach number and air density, so appropriate corrections to those characteristics as listed in Table 2 of Part 1 should be made. Alternately (and better), the transfer function can be determined for the actual flight conditions using the approach from Part 1. For a representative transfer function, see Fig. 1 from Part 1.

2. Calculate the air temperature T_a:

   (a) Method 1: Because the transfer function is the ratio between Fourier representations of the output and the input, the Fourier transform ($(\hat{T}_r(\nu))$ of the input recovery temperature $(T_r(t))$ will be $\hat{T}_m(\nu)/H(\nu)$, where the circumflex ($\hat{}$) denotes the Fourier transform, so the recovery temperature can be retrieved using the inverse Fourier transform of $\hat{T}_m(\nu)/H(\nu)$. The air temperature then is calculated from $T_r - Q'$ where $Q'$is the result of filtering the dynamic heating term Q using the response characteristic of the sensor. Q' can be found from the inverse Fourier transform of $H(\nu)\hat{Q}(\nu)$.

   (b) Method 2: Use the differential equations to find T_r from the measurements T_m, as in Sect. 4.1 of Part 1. Filter the dynamic heating to obtain Q' as specified in Part 2. Then $T_a = T_r - Q'$.

3. The cospectrum then is calculated for the cross-spectrum of temperature and updraft, with a choice made regarding which frequency interval to include. This will normally exclude wavelengths longer than a few kilometers.

4. Finally, calculate the flux from the sum of the resulting cospectrum over the specified frequency interval.

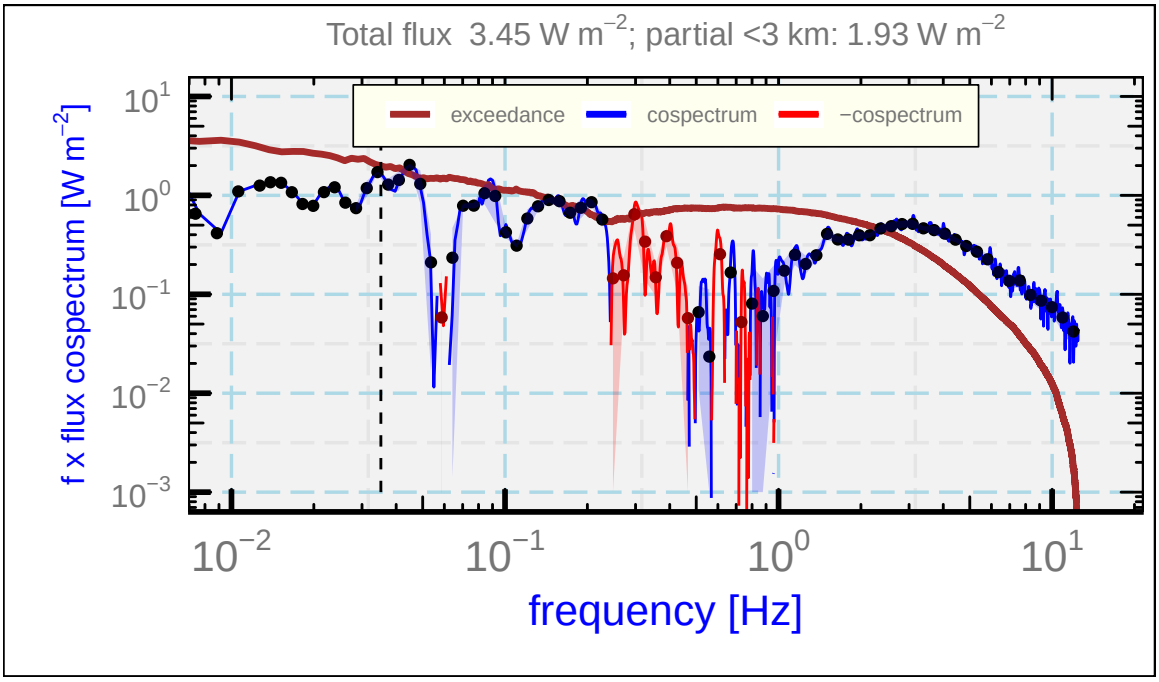

Figure 1: The cospectrum for temperature and updraft, multiplied by the air density and specific heat to convert to a cospectrum for the sensible-heat flux, for six 10-min boundary-layer flight segments from the VOCALS project. The original uncorrected measurements have been used for temperature. Positive and negative values of the cospectrum are shown as blue and red, respectively, with the sign of the latter changed to permit plotting on a logarithmic axis. The mean values in logarithmically spaced bins in frequency are shown as black and dark red dots, and the shaded ribbon enclosing the dots represents a one-standard-deviation range for those bins. The brown line labeled "exceedance" is the complement of the cumulative distribution function for flux; i.e., the flux from all frequencies higher than the plotted value. The dashed black line denotes the frequency that corresponds to a wavelength of 3 km.

2 Examples with Corrections Applied

2.1 VOCALS example

The same flight segments from the VOCALS project that were used to characterize the transfer function in Part 1 are also used in this first example. A composite cospectrum for these measurements was constructed as before, averaging six 10-min boundary-layer flight segments of 25 Hz measurements of recovery temperature, updraft, and dynamic heating. This first calculation used the measurements directly, with no corrections for the response of the temperature sensor and no adjustment of the dynamic-heating correction, so this would be the conventional measurement without any of the changes proposed in the present series of papers. The cospectrum for the cross-spectrum between temperature and updraft is shown in Fig. 1 for the average of the six flight segments.

This plot format is unconventional and so needs some explanation because it will be used as the primary display of the cospectrum in this paper. The cospectrum can be positive or negative, so it is often plotted using a linear scale for the abscissa. However, as the figure shows, the range of ordinate values is displayed better with a logarithmic scale, even after weighting the cospectrum by frequency. The compromise made in this plot is to use a logarithmic scale but plot negative values with sign reversed and with a different color, here red instead of blue. The values plotted in red therefore should be regarded as negative values of the plotted magnitude. There is then a dead-band at the bottom of the plot where spectral values with very small absolute value lie, here absolute values smaller than $10^{-3}\,\mathrm{W\,m^{-2}}$. A plot weighted by frequency is used as is appropriate for a logarithmic abscissa. There are several other features of this plot:

1. The cospectrum (blue line) has been smoothed using Daniell smoothing, with consecutive smoothing using width-3 for frequencies above 0.01 Hz, then width-5 for frequencies above 0.1 Hz, then width-17 for frequencies above 1 Hz. For these 10-min flight legs and for 25 Hz measurements, the maximum smoothing interval corresponds to a smoother spanning about 0.025 Hz, so most spectral features are retained even with this strong smoothing. Additional smoothing results from averaging six cospectra to obtain the plotted values.

2. Further smoothing is included by binning the results into 100 logarithmically spaced intervals in frequency and averaging in those bins. That results in the blue dots (or dark red dots for negative points).

3. A shaded ribbon denotes the standard deviation of the values in the bins. In many cases it is too narrow to be visible.

4. The total flux indicated in the title is that arising from the part of the flux with frequency above 0.01 Hz. This corresponds to a wavelength of more than 10 km for the C-130 and more than 15 km for the GV. In addition, there is another estimate of the contribution to the flux from wavelengths below a selected limit, here 3 km. That or a still smaller wavelength limit is often a reasonable estimate of the part of the flux contributed by turbulent air motions in the boundary layer, so that will be regarded as the primary measurement of sensible-heat flux.

5. One additional line is plotted brown and labeled "exceedance." That is a cumulative distribution function for the cospectrum, called "exceedance" because it is the complement of the conventional cumulative distribution: It shows the contribution from all frequencies higher than the indicated value. That is more informative at high frequency on a logarithmic scale, where some of the most interesting variation is located. Unlike the other plotted values, its units are $\mathrm{W\,m^{-2}}$, not $\mathrm{W\,m^{-2}}$ per logarithmic interval as is the case for the weighted cospectrum.[1]

Although the value measured for the sensible-heat flux is small, the plot indicates that there are positive contributions to the flux up to the highest frequencies measured. The

[1]The cumulative distribution termed "exceedance" here is sometimes called the ogive.

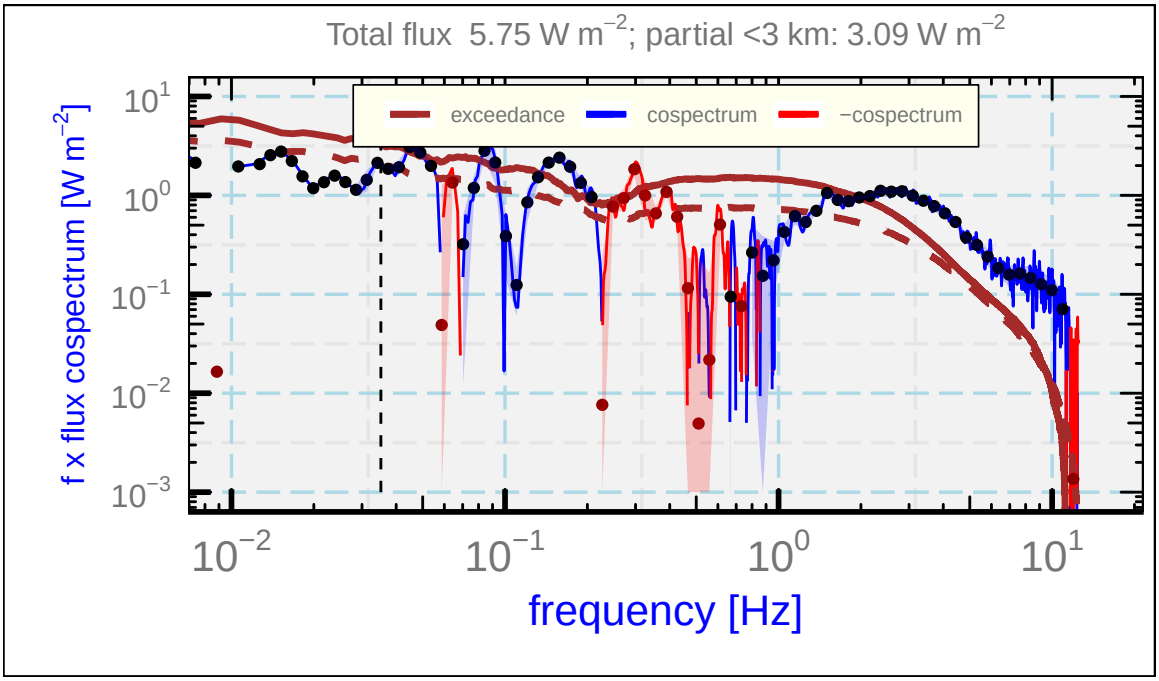

Figure 2: The cospectrum for temperature and updraft, multiplied by the air density and specific heat to convert to a cospectrum for the sensible-heat flux, for six 10-min boundary-layer flight segments from the VOCALS project. The measurements used in the preceding plot have been corrected for the time response of the temperature sensor, and the dynamic-heating correction has been filtered to compensate for the expected response of the temperature sensor. Further description of the plot is included in the caption for the preceding figure. An added line is the dashed brown line; it duplicates the exceedance plot from the uncorrected calculation of the cospectrum as shown in the previous figure.

adjustment in dynamic heating has only a minor (ca. +10%) effect on the measured flux, but it is not negligible. It is an encouraging sign that there seems to be some consistent contribution to the flux even from the high-frequency range.

The result after corrections for the time response of the sensor is shown in Fig. 2. The exceedance distributions for the original and corrected measurements of sensible-heat flux are both shown in this figure, the former as the dashed brown line. For this plot, the combination of the correction methods described in Sect. 1.2 was used by correcting the measured temperature for dynamic heating using the digital filter but then using Fourier transforms to find the corrected flux as specified by the transfer function. Only minor differences arose when the other combinations of the methods were used. The estimated flux of sensible heat is increased by about 60%, from 1.93 to 3.09 W m^{-2} for the contribution to the flux from wavelengths smaller than 3 km, and the flux attributable to frequencies above 1 Hz increased by 100%.

The VOCALS data led to very small sensible-heat flux. (For comparison, solar insolation provides a top-of-the-atmosphere flux of more than 1000 W m^{-2}. The measured flux of

sensible heat in this case is insignificant, although the measurement itself appears valid.) Therefore it is useful to extend these measurements to cases with more flux of sensible heat.

2.2 SOCRATES example

Flight 15 from the "Southern Ocean Clouds, Radiation, Aerosol Transport Experimental Study" (SOCRATES), from 24 January 2018, 6:00:00 to 6:15:00 UTC, was another flight segment at low level over the ocean on which the unheated Rosemount sensor was used to measure temperature. The same procedure was followed as for VOCALS, with two changes: The flight was split into three 5-min flight segments and the results from those segments were averaged when the cospectrum was calculated, and the transfer function used was that determined based on GV measurements from this same project and flight, as listed in Part 1 Table 2.

Figure 3 shows the measured cospectrum leading to the measured flux of sensible heat listed in the plot title. The exceedance distribution before correction, shown as the dashed brown line, was calculated using a dynamic-heating correction that was filtered to match the response of the sensor, but otherwise was not corrected. Without correction for the response as represented by the transfer function, about 30% of the flux of sensible heat would be missed. The underestimation is particularly serious at higher frequencies: The measured contribution from frequencies above 1 Hz is about twice as large after correction as it is without correction. Lawson and Rodi [1992] estimated that, in comparison to their fast thermocouple sensor on a slower aircraft, the unheated Rosemount sensor underestimated the flux by about 21% in their measurements. The magnitude of the correction applied here is thus reasonably consistent with expectations from their study.

By obtaining a realistic measurement of the cospectrum at high frequency, it is possible to estimate how much of the otherwise unknown contribution above 1 Hz has been missed and therefore to judge if the frequency coverage is adequate. In this case, the exceedance curve is less than 2% at 10 Hz and falls rapidly above that frequency, so it appears likely that additional contributions from higher frequencies can go unmeasured without introducing serious errors into the measurement of flux.

Appendix A presents simulation results that support these methods used to calculate corrections to the flux. These results in combination with those presented in this section indicate that defensible measurements of the flux of sensible heat can be made using the unheated Rosemount 102E4AL sensor if the measurements are corrected for the time response of the sensor.

2.3 CSET example

The "Cloud Systems Evolution in the Trades" (CSET) experiment included many low-level (150 m) flight segments over the Pacific Ocean between California and Hawaii, USA, and an unheated Rosemount 102E4AL sensor was flown on the NSF/NCAR GV during this

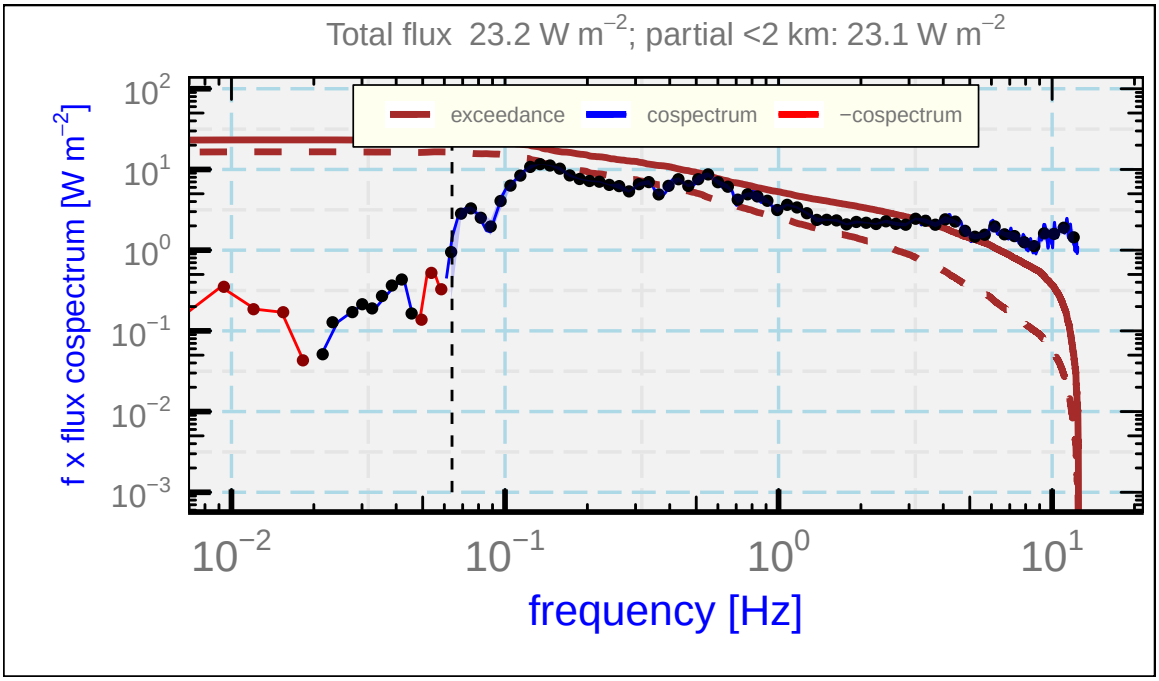

Figure 3: The corrected flux of sensible heat for SOCRATES flight 15, 6:00:00 to 6:15:00, a low-level flight segment over the southern-hemisphere ocean. The "exceedance" is the complement of the cumulative distribution function (i.e., the sum of contributions from frequencies above the plotted value), and the dashed brown exceedance line is that without transfer-function correction but with adjustment of the dynamic-heating term to incorporate the estimated response of the temperature sensor.

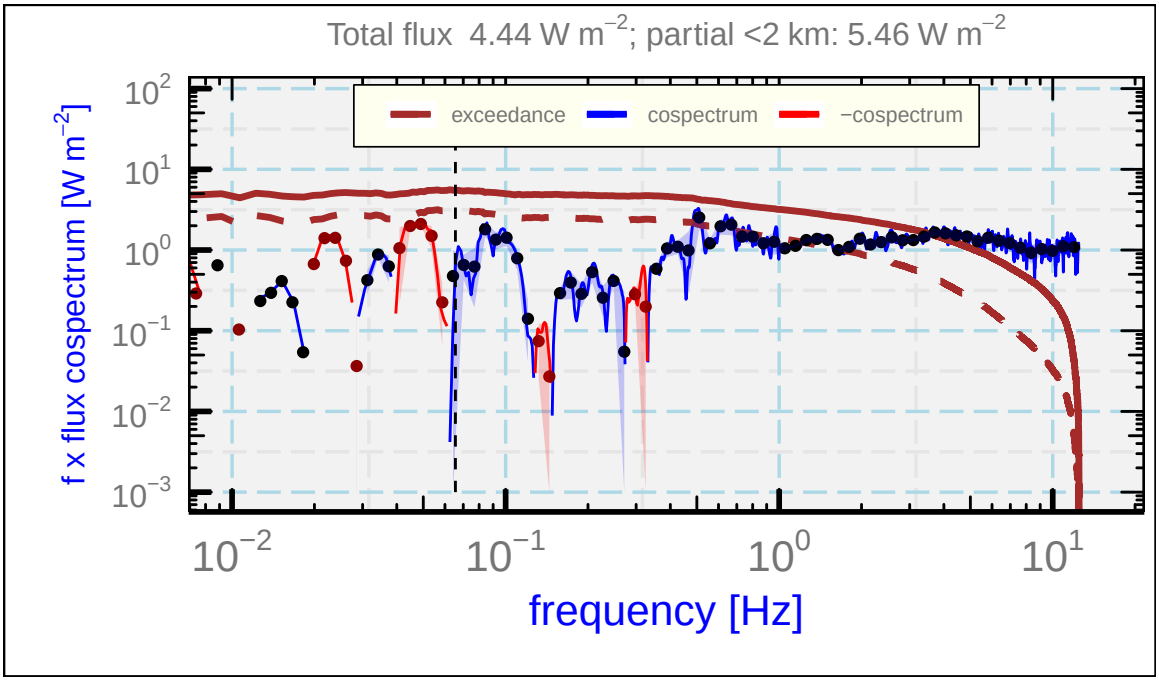

Figure 4: Cospectrum for the flux of sensible heat, for three 10-min flight segments from the CSET project. The dashed brown line is the exceedance distribution before correction, which gives a flux of 3.07 W m−2 for wavelengths smaller than 2 km and 2.06 W m^{-2} for frequencies above 0.01 Hz.

project. These measurements provide another opportunity to evaluate the measurements of sensible-heat flux. Three low-level flight segments were selected from research flight 5 (14 July 2015): 17:52:00 to 18:02:00, 19:45:30 to 19:55:30, and 20:37:17 to 20:47:17. The procedure was the same as used for the preceding SOCRATES example: Calculate the air temperature with a dynamic-heating correction filtered to match the sensor response, then average the cospectra of air temperature and updraft for the three segments so that the uncorrected and corrected measurements of flux can be compared..

The resulting cospectrum is shown in Fig. 4. Without correction, the measured flux would be about 56% of the corrected flux for wavelengths smaller than 2 km, and for fluctuating frequencies above 1 Hz the measured flux would be only about 43% of that obtained from the corrected measurements. The indication from this example, as from the others, is that the correction can amount to a significant part of the measured flux and that, without correction, the flux would be underestimated by around 50%.

3 Summary and Conclusions

Some key conclusions from Parts 1 and 2 are included briefly here so that this summary can encompass all three papers. The key findings are these:

1. In Part 1, a transfer function for an unheated Rosemount 102E4AL sensor was determined and shown to be consistent with constraining measurements. A parametric representation depending on three parameters was shown to lead to reasonable correction of the measurements of recovery temperature.

2. Part 2 argued that, because temperature sensors often do not respond fast enough to measure high-frequency components of the dynamic-heating correction, erroneous corrections are introduced by conventional data processing. Instead, the corrections should be filtered to match the response of the temperature sensor to avoid introduction of these errors.

3. In this Part 3, a correction procedure was proposed that consists of using the transfer function from Part 1 and the modified correction for dynamic heating developed in Part 2 to calculate the sensible-heat flux. Three cases are presented, all with significant correlation between temperature and updraft at a range of frequencies including those above 1 Hz. The measured values of sensible-heat flux would be underestimated significantly (by about 40%, 30%, and 44% in the three cases) without correction.

4. The cospectrum with correction appears to be represented reasonably at frequencies up to about 10 Hz, so the rapidly decreasing concentration to the cospectrum from these frequencies suggests that it is not necessary to measure contributions from frequencies above this limit. This conclusion is tentative and needs reconsideration when applied to new cases.

5. These results are reproducible using the document that generated this report, and this report is archived along with appropriate data sources so that they will be accessible to others who might want to apply these approaches to other sensors or use these correction schemes to improve measurements of the flux of sensible heat. Appendix B provides specific information to aid an analyst who might want to replicate or extend this study. In particular, an accompanying "workflow" statement provides additional details and documents some additional aspects of the study that are not included in this report, and methods to access the data used are included in that workflow document.

A Appendix: Assessment Via Simulation

A.1 The Goal

This appendix uses simulated measurements with the analysis methods developed in this paper to demonstrate that those correction schemes can recover the assumed simulated conditions. Toward this end, it is useful to generate time series representing isotropic wind measurements that have a specified relationship to the eddy dissipation rate and the expected $-5/3$ slope of spectral variance vs. frequency that is expected for an inertial sub-range. The code used here generates such a time series of duration $T = 30\,\text{min}$ by generating a Gaussian-noise spectrum, finding the Fourier transform, weighting the components to obtain a $-5/3$ slope, and then using an inverse Fourier transform to reconstruct a simulated measurement series representing an inertial subrange. To provide a more realistic representation of the variance spectra often observed, the spectral variance is attenuated a low frequency to produce a peak variance at several-kilometer wavelength.

The variance spectrum expected for an inertial sub-range has the following form:

$$P(\nu) = C \left(\frac{2\pi}{V}\right)^{-2/3} \epsilon^{2/3} \nu^{-5/3} \tag{2}$$

where $C = 0.5$ for the longitudinal component of the wind and $2/3$ for a lateral component. An eddy dissipation rate of $10^{-3}\,\text{m}^2\text{s}^{-3}$ and a flight speed of $V = 200$ m/s were used with (2) to specify the desired variance spectrum.

The result for one realization of the time series is shown in Fig. 5. The match to the assumed eddy dissipation rate ($10^{-3} m^2 s^{-3}$) is good. When calculating the simulated flux, the very-long-wavelength components (with frequency below 0.02 Hz) were attenuated before the series was used. This seemed to improve the accuracy of the high-frequency simulation, which otherwise exhibited some variability for different random sequences but became more consistent with this adjustment.

A.2 Simulated Flux

To determine how a simulated time series would be measured, it was necessary to generate two realistic time series for the updraft and the temperature. To produce a flux, there should be some correlation between these so that the measurement based on (1) will be non-zero. Therefore, the two time series were generated as follows:

1. A time series for w' was generated that has eddy dissipation rate of $10^{-3}\text{m}^2\text{s}^{-3}$, as shown in Fig. 5.

2. A second independent time series T with fluctuations T' scaled smaller by a factor of five was generated to represent the *air* temperature.

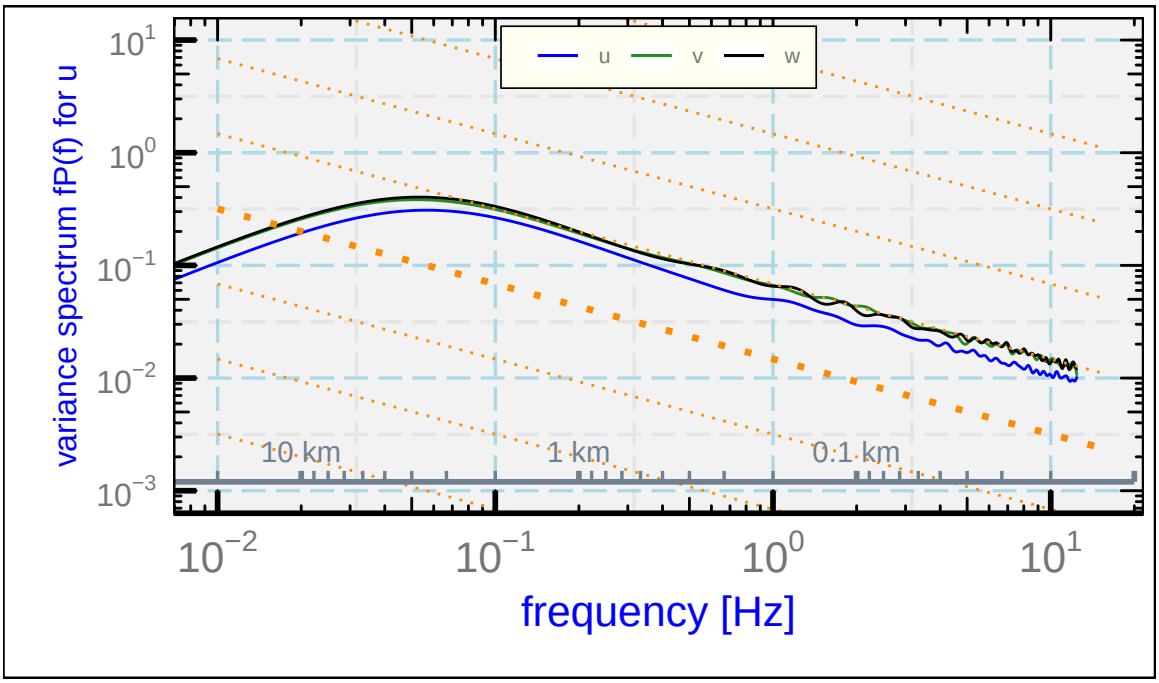

Figure 5: The variance spectrum of the generated time series. Three wind components are shown: u longitudinal; v side lateral; w upward. The simulated eddy dissipation rate was 10^{-3} m^2s^{-3}. *The generated longitudinal spectral density (u) is 3/4 the lateral spectral densities (v and w), as expected in an inertial subrange. The dashed orange lines indicated the expected slope (*$-2/3$ *for this distribution because it is weighted by frequency), with the large-dot line representing* 10^{-4} m^2s^{-3} *and other lines representing eddy dissipation rates factors of 10 higher or lower. The spectral variance has been attenuated at low frequency to simulate the shapes that are often observed. The displayed wavelength scale was determined from the average flight speed.*

3. Correlation between the two time series was then introduced by defining a new temperature time series with the fluctuations $T'_c = (1-r)T' + rw'/5$ where $r = 0.3$. The result will be $< w'T'_c >= r\sqrt{\sigma_w \sigma_{T_c}}$, which will lead to a flux of sensible heat specified as

$$F_s = \rho_a C_p r \sqrt{\sigma_w \sigma_{T_c}}$$

An example is shown in Fig. 6. In this simulation, the correlation is the same at all frequencies so the contribution to the measured flux also extends over all frequencies, with decreasing contributions as frequency increases. In this case, about 10% of the < 5 km flux is contributed at frequencies above 1 Hz, where there is danger that the real sensor will respond incompletely to the fluctuations. The potential effects of the sensor response and possibly incorrect adjustment for dynamic heating can then be determined by replacing the dynamic-heating term with the filtered version as specified in Part 2 and then by calculating the expected measurement by filtering the recovery temperature in the same way.

A.3 Application of corrections

Figure uncorrected measurement of temperature used to generate Fig. 7 results from digital filtering to correct the dynamic heating term but otherwise without correction based on the transfer function. To be specific:

1. A true recovery temperature T_r was calculated by adding the dynamic-heating term Q to the simulated air temperature T.

2. The digital filter for the unheated Rosemount sensor as determined from measurements on th GV, with response characteristics as listed in Table 2 of Part 1, was applied to T_r to obtain an estimate of the time series that would be measured, T_m.

3. The same digital filter was applied to the dynamic-heating term Q to obtain an estimate of how the sensor should respond to that dynamic heating, denoted here as Q'.

4. That estimate of the probe response to dynamic heating was subtracted from T_m to obtain a prediction of the air temperature that would be measured, $T_a = T_m - Q'$.

5. The flux was then calculated from (1) using T_a and the simulated updraft. That produced the uncorrected flux characterized by the dashed brown line in Fig. 7.

6. The correction procedure from Sect. 1.2 was then used to correct for the flux of sensible heat that would be missed because the temperature sensor does not respond instantly.

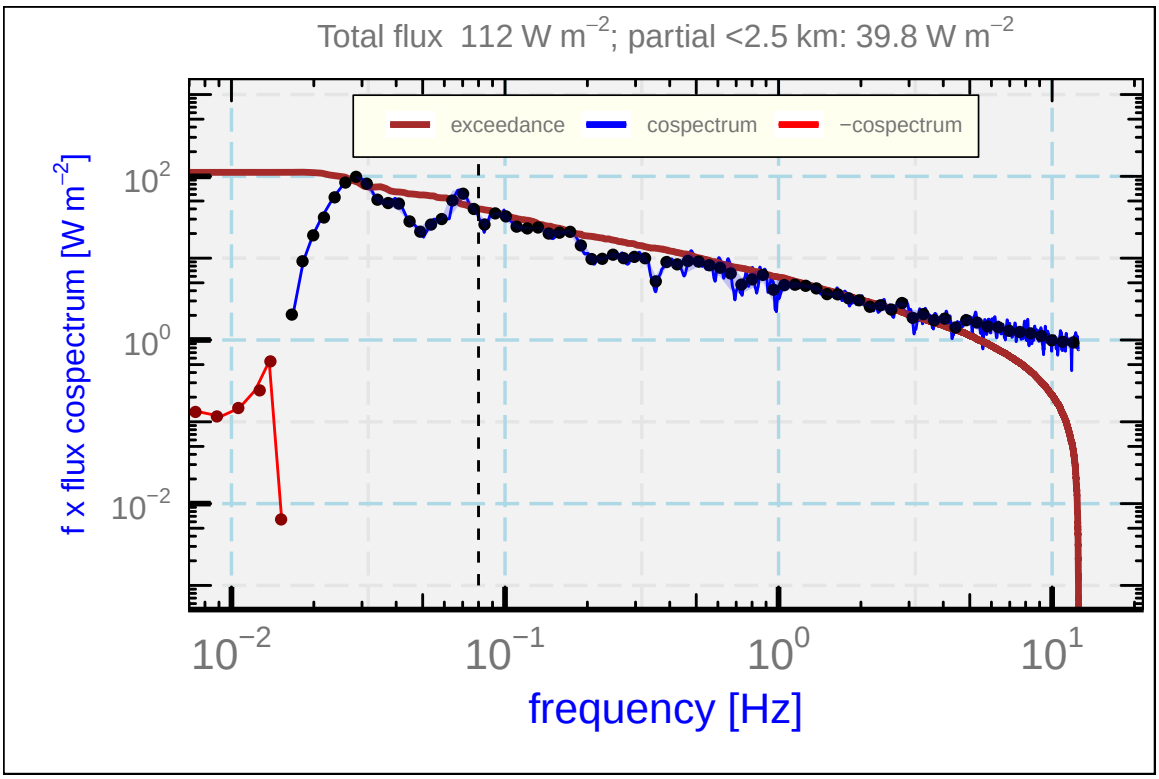

Figure 6: The cospectrum for the flux of sensible heat for the simulated data generated as described in the text. Three 10-min segments of simulated 25 Hz data, with 0.3 correlation coefficient between fluctuations in temperature and updraft and the correlated fluctuations in temperature scaled to have amplitude 20% of those in updraft.

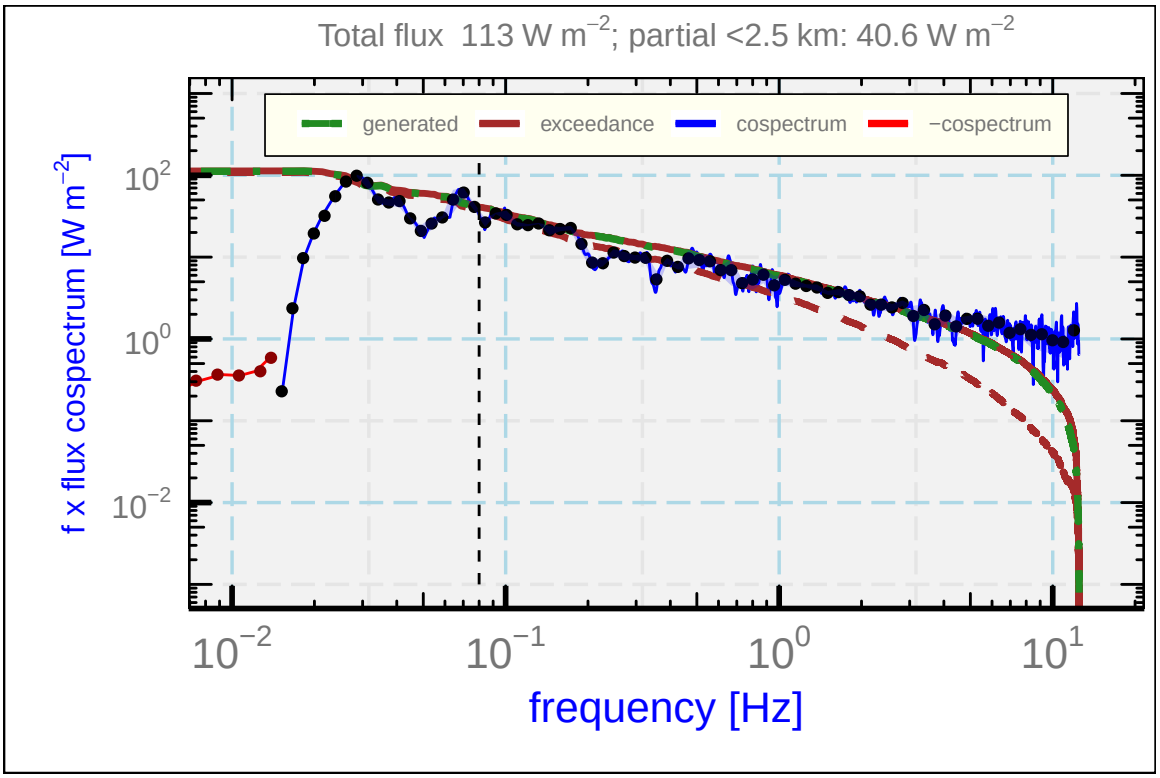

Figure 7: The cospectrum for the flux of sensible heat for the simulated measurement of a realistic sensor (here, the unheated Rosemount 102E4AL sensor) with the revised dynamic-heating correction (Q') and the measurement calculated by applying the digital filter from Part 2 to the assumed recovery-temperature history as simulated. The correction procedure from Sect. 1.2 was used to estimate the corrected flux shown as the plotted spectrum and the solid brown exceedance distribution. The dashed exceedance line is the uncorrected result, for which the contributions from frequencies above 1 Hz are only 3.4 W m^{-2} vs. 5.9 W m^{-2} for the cospectrum as generated.

The result was remarkable consistency between the generated flux (39.8 $\mathrm{W\,m^{-2}}$) shown in Fig. 6 and the flux estimated after the correction procedure (40.6 $\mathrm{W\,m^{-2}}$) as shown in Fig. 7. The representation of the high-frequency contribution is improved significantly by the correction procedure, and the exceedance distributions are almost identical for the generated and corrected cospectra, as shown by the agreement between the corrected exceedance distribution (solid brown line) and the generated exceedance distribution (dashed green line) in Fig. 7. Thus, the simulation supports both the correction procedure from Sect. 1.2 and the proposed treatment of dynamic heating in Part 2. Of course, this does not demonstrate that the fitted transfer function is correct as determined in this document, only that the use of that transfer function and the digital filter derived from it are consistent.

B Reproducibility

This document is constructed in ways that support duplication of the study. The code that generates the plots and implements the correction procedure is incorporated into the same file that generated this document via LaTeX, using principles and techniques described by Xie [2013] as implemented in the R package 'knitr' (Xie [2014]). The program, 'SensibleHeatFluxPaper1.Rnw', is archived on 'GitHub' in the directory at this URL. There is some supplemental material in that directory, including the workflow document, the bibliography and some code segments saved in the "chunks" subdirectory, so the full directory should be downloaded in order to run the program. The calculations use the programming language R (R Core Team [2019]) and were run within RStudio (RStudio [2009]), so this is the most straightforward way to replicate the calculations and the generation of this document.

A package named Ranadu, containing auxillary functions, is used extensively in the R code. It is available on GitHub as https://github.com/WilliamCooper/Ranadu.git. The version used for calculations in this technical note is included in the 'zip' archive listed below.

The data files used are also preserved in the NCAR/EOL Data Archives and can be obtained via a request to `mailto:raf-dm@eol.ucar.edu` or via the "Data Access" links at this web site. The original files containing the data as produced by the NCAR Earth Observing Laboratory, Research Aviation Facility, were in netCDF format (cf. this URL), but in many cases data archives were reprocessed and the files may change after reprocessing so a separate archive is maintained for this document. The data files in this archive contain R data.frames and are preserved as binary-format 'Rdata' files via R 'save' commands. The code in the GitHub archive has appropriate 'load' commands to read these data files from a subdirectory named 'Data' (/Data or ~/Data or /home/Data) but this is not part of the GitHub repository because it is too large to be appropriate there. To reproduce this research, those data files have to be transferred separately from {??where??}

Extensive use has been made of attributes assigned to the data.frames and the variables in those data.frames. All the attributes from the original netCDF files have been transferred, so there is a record of how the original data were processed, for example recording calibration coefficients and processing chains for the variables. Once the data.frames are loaded into R, these attributes can be viewed and provide additional documentation of what data were used. Key information like the processing date, the program version that produced the archive, and the selection of primary variables for various measurements thus is preserved.

(See the related list of project components on the next page that are preserved to enhance reproducibility.)

PROJECT:	SensibleHeatFlux
ARCHIVE PACKAGE:	SensibleHeatFluxPaper3.zip
CONTAINS:	attachment list below
PROGRAM:	SensibleHeatFluxPaper3.Rnw
ORIGINAL DATA:	UCAR/NCAR - Earth Observing Laboratory [2011], UCAR/NCAR - Earth Observing Laboratory [2019], UCAR/NCAR - Earth Observing Laboratory [2017]
SPECIAL DATA FILES:	SensibleHeatFluxTechNote.Rdata, SensibleHeatFluxTechNote2.Rdata
WORKFLOW DOCUMENT:	WorkflowSensibleHeatFluxPaper3.pdf
GIT:	https://github.com/WilliamCooper/SensibleHeatFlux.git

Attachments:
SensibleHeatFluxPaper3.Rnw
SensibleHeatFluxPaper3.pdf
WorkflowSensibleHeatFluxPaper3.pdf
WAC.bib
chunks/*
SessionInfo

References

Berend Hasselman. *nleqslv: Solve Systems of Nonlinear Equations*, 2018. URL https://CRAN.R-project.org/package=nleqslv. R package version 3.3.2. (document)

R. Paul Lawson and Alfred R. Rodi. A new airborne thermometer for atmospheric and cloud physics research. part i: Design and preliminary flight tests. *Journal of Atmospheric and Oceanic Technology*, 9(5):556–574, 1992. doi: 10.1175/1520-0426(1992)009<0556:ANATFA>2.0.CO;2. URL https://doi.org/10.1175/1520-0426(1992)009<0556:ANATFA>2.0.CO;2. 2.2

David Pierce. *ncdf4: Interface to Unidata netCDF (Version 4 or Earlier) Format Data Files*, 2015. URL https://CRAN.R-project.org/package=ncdf4. R package version 1.15. (document)

R Core Team. *R: A language and environment for statistical computing*. R Foundation for Statistical Computing, Vienna, Austria, 2019. URL http://www.R-project.org. (document), B

RStudio. *RStudio: Integrated development environment for R (Version 0.98.879)*, 2009. URL http://www.rstudio.org. (document), B

Bruce Swihart and Jim Lindsey. *rmutil: Utilities for Nonlinear Regression and Repeated Measurements Models*, 2019. URL https://CRAN.R-project.org/package=rmutil. R package version 1.1.3. (document)

UCAR/NCAR - Earth Observing Laboratory. NCAR/NSF C-130 navigation, state parameter, and microphysics HRT (25 sps) data. version 1.0 [data set, VOCALS], 2011. URL https://doi.org/10.5065/d69k48jk,Accessed09Jan2020. (document), B

UCAR/NCAR - Earth Observing Laboratory. High rate (hrt - 25 sps) navigation, state parameter, and microphysics flight-level data. version 2.0. [data set, CSET], 2017. URL https://doi.org/10.5065/D63R0R3W,Accessed12Mar2020. B

UCAR/NCAR - Earth Observing Laboratory. High rate (HRT - 25 sps) navigation, state parameter, and microphysics flight-level data. version 0.1 [preliminary] [data set, WE-CAN], 2018. URL https://data.eol.ucar.edu/dataset/548.004. Accessed09Jan2020. (document)

UCAR/NCAR - Earth Observing Laboratory. High rate (HRT) navigation, state parameter, and microphysics flight level data. version 1.0 [data set, SOCRATES], 2019. URL https://doi.org/10.26023/K5VQ-K6KY-W610,Accessed09Jan2020. (document), B

H. Wickham. *ggplot2: elegant graphics for data analysis*. Springer New York, 2009. ISBN 978-0-387-98140-6. URL http://had.co.nz/ggplot2/book. (document)

Y. Xie. *Dynamic Documents with R and knitr*. Chapman and Hall/CRC, Boca Raton, Florida, 2013. URL http://yihui.name/knitr/. ISBN 978-1482203530. (document), B

Y. Xie. *knitr: A general-purpose package for dynamic report generation in R*, 2014. URL http://yihui.name/knitr/. R package version 1.6. (document), B